Confrontation of heat transport models against Tore Supra and JET high performance discharges

G.T. Hoang, J.F. Artaud, V. Basiuk, A. Bécoulet, L.G. Eriksson, C. Fourment, W. Horton*, G. Huysmans, F. Imbeaux , X. Litaudon, D. Mazon, D. Moreau, Y. Peysson.

Association CEA-Euratom sur la Fusion, CEA/DSM/DRFC,
CEA Cadarache, 13108 St Paul-Lez-Durance, FRANCE
e-mail: tuong.hoang@cea.fr
** Present address: Institute for Fusion Studies. The University of Texas at Austin, Austin, Texas 78712, USA*

Abstract

Some theoretical and empirical heat transport models are tested against a wide database of discharges heated by fast wave electron heating (FWEH) scheme and discharges with combined auxiliary heating schemes (NBI, ICRH, LHCD) exhibiting both the ion and electron internal transport barrier (ITB). The results of the electron transport analysis strongly favor a model based on the electromagnetic turbulence driven by electron temperature gradient (ETG).

I. Introduction

This work is devoted to both the interpretative and predictive transport studies of advanced tokamak regimes in Tore Supra and JET, using various (ion and electron) heating methods.
For this purpose, we use the improved version of the CRONOS code [1]. In Sec. II, the CRONOS code is briefly described. Electron heat transport models (Mixed Bohm/gyro-Bohm [2], Rebut-Lallia-Watkins [3], Weiland-Nordman [4] and ETG [5]) are tested against the Tore Supra FWEH discharges in Sec. III. In Sec. IV, a JET discharge, using LHCD power during the current ramp-up, exhibiting the ion and electron ITBs is simulated interpretatively. In Sec. V, a pure predictive simulation of a Tore Supa discharge heated by fast wave is reported.

II. Description of the CRONOS code

The CRONOS code couples the diffusion equations to a 2-D equilibrium code (HELENA, [6]). It deals with any kind of equilibrium (circular, X-points, high triangularity, …), performing the full link between flux averaged quantities and the equilibrium. Such a feature allows us to directly couple CRONOS to MHD stability codes, and to micro-turbulence analysis codes. The integrated package codes solve in a fully self-consistent manner the whole system of transport equations together with the current diffusion equation, the plasma equilibrium and the sources (i.e. heat, particle and non-inductive current) for multiple species plasmas. This feature, which differs from the existing codes, therefore allows us to test the various heat transport models, consistently with the heat flux calculations, against the experiments. Consistent calculation is required, since there are feedback and feedforward couplings between these quantities. In particular for plasmas with LHCD, the LH power depositon profile is non-linearly coupled to the current density profile and transport. Various modules calculating the sources are detailed in Table I.

Table I

Source	Code
Bootstrap current	NCLASS [7]
LHCD	i) DELPHINE Ray-tracing / 2-D Fokker-Planck code [8]
	ii) Hard X-rays measurements.
NBI	SINBAD [9] or Monte Carlo (TRANSP)
ICRH	i) Minority scheme: PION [10]
	ii) Direct electron heating: ABSOR [11]
	iii) Current drive: simple analytical model
ECRH	REMA [12]

III. Comparison of electron transport models against the Tore Supra FWEH discharges

We use a series of shots with increasing T_e in response to the fast wave power P_{FW}, having the same density n_e and q profiles (Fig. 1), carried out in TS at plasma current I_p = 0.6 MA and toroidal field B = 2.2 T. For each radial position, the variations (less than 10%) of n_e and q are smaller than their absolute error bars. The range of the total power is 1.5-7.5 MW (Ohmic power P_{OH} = 0.1 - 0.75 MW and P_{FW} = 0.75 -7.4 MW). These plasmas, with dominant electron heating, exhibit an improvement of confinement, linked to peaked current density profile (high plasma inductance) due to the large fraction of bootstrap current mainly generated by peaked electron temperature profile. Thermal energy confinement time is found to exceed the L-mode prediction by a factor of 1.7 (2.2 on electron channel). From this data 21 time slices in the stationary phases of 8 discharges were selected. The large variation of P_{FW} allows an accurate scan of the electron temperature gradient from 1 keV/m to 12 keV/m.

Four following electron models have been tested:

i) Taroni Mixed Bohm/gyro-Bohm [2] $\chi_e^{B/gB} = \chi_e^B + \chi_e^{gB}$ (Eq. 1)

where $\chi_e^B = 8.10^{-5} q^2 \frac{T_e}{B} \frac{a}{L_{pe}} \left|\frac{\nabla T_e}{T_e}\right|_{edge}$ and $\chi_e^{gB} = 710^{-2} \frac{T_e}{B} \rho^* \frac{a}{L_{Te}}$

ii) Rebut-Lallia-Watkins (RLW) [3],

$$\chi_e^{RLW} = 2\sqrt{T_e/(T_e+T_i)}(1-\sqrt{r/R})\frac{1}{B\sqrt{R}}\frac{q^2}{\nabla q}\left(\frac{\nabla T_e}{T_e} + 2\frac{\nabla n}{n}\right)\left(1-\frac{\nabla T_c}{\nabla T_e}\right) \quad \text{(Eq. 2)}$$

where $(\nabla T_e)_c^{RLW} = \frac{6}{q}\sqrt{\eta j B^3 / n_e T_e^{1/2}}$

iii) Weiland-Nordman, solving a 5x5 transport matrix, including the electromagnetic effects and electron trapping,

iv) Horton ETG model, based on the electromagnetic turbulence driven by ETG and collisionless electron skin depth [5],

$\chi_e^{em} = C_{em} q^{\nu} \frac{c^2}{\omega_{pe}^2} \frac{v_e}{(L_T R)^{1/2}} \left(\frac{R}{L_T} - \frac{R}{L_c}\right)$ (Eq. 3), where $\frac{R}{L_c} = 1.88\frac{|s|}{q}(1+Zeff\frac{T_e}{T_i})$ and C_{em}=0.1

We limit our analysis to normalized radius (r/a) between 0.2 and 0.75, since the plasma center is dominated by the heating source and the power balance at the edge is affected by uncertainties from radiation and recycling. Comparison of power balance analysis with the above electron models is illustrated in Fig. 2. The considered models can qualitatively simulate the experimental results with some restrictions. However, the electromagnetic ETG model in Eq. 3 is found to be better for the turbulent electron thermal diffusivity modeling than the other ones, except for low injected power cases (especially ohmic regime) in which the predicted critical gradient is too high. Mixed Bohm/gyro-Bohm model over estimates χ_e. It can simulate the profile of χ_e by decreasing the Bohm term χ_e^B in Eq. 1: it must be divided

by a factor of 2. A disagreement is also appears in electron temperature gradient dependence when ∇T_e>5-6 keV/m. RLW model is better to simulate the temperature gradient and magnetic shear effects. However, the plasma parameter dependence in $(\nabla T_e)_c^{RLW}$ formula is not correctly described. The Weiland-Nordman model can reproduce the experimental χ_ePB profile by fixing $k\rho_\theta$ = 0.03 and taking into account the electromagnetic effect. The comparison of the above electron models with the power balance analyses is illustrated in Fig. 2. In this comparison, no critical gradient is considered in both the RLW and ETG models, and the χ_e^B term in Eq. 1 is divided by 2.

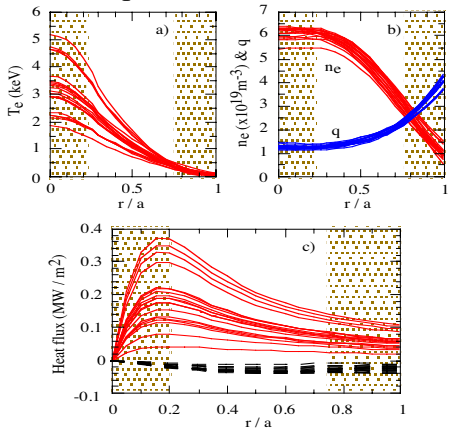

Fig. 1: (a) Electron temperature, (b) electron density and safety factor, (c) heat flux (solid lines: FW coupled to electrons + Ohmic; dashed lines: radiation and electron-ion losses).

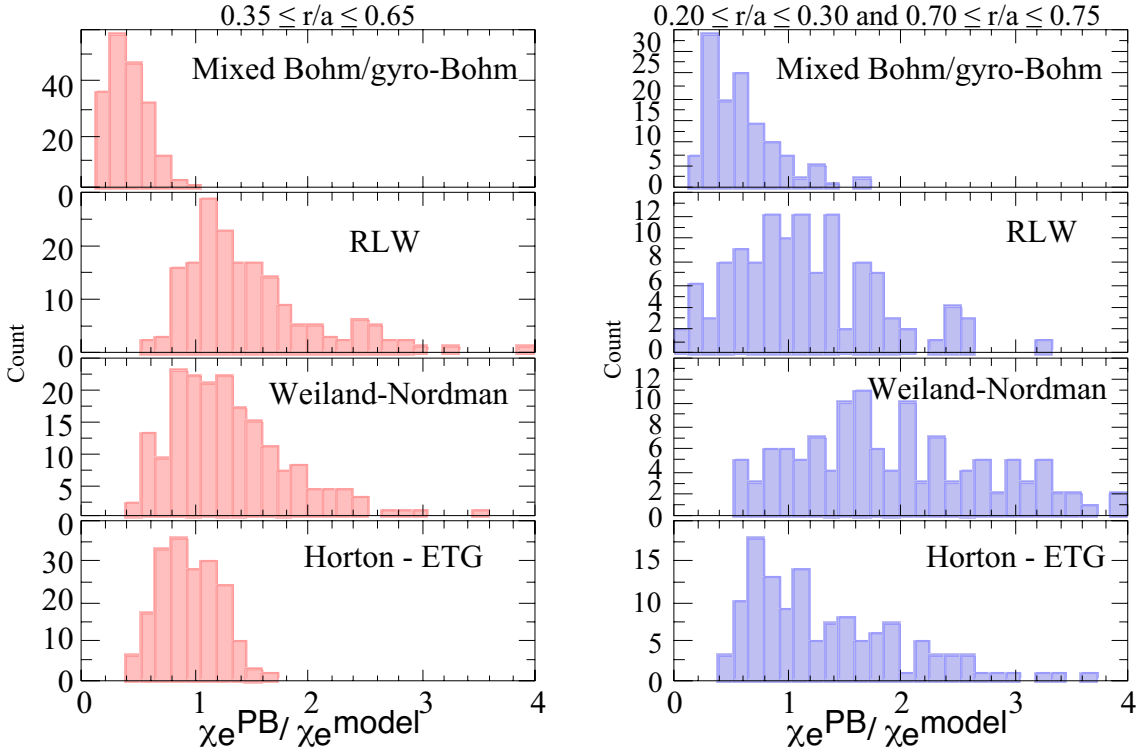

Fig. 2: Comparison of power balance analyses with various electron transport models. 252 entries (12 radial positions x 21 time slices; n_e = 2.5 - 6.5x$10^{19}m^{-3}$, T_e = 0.3 - 5.5 keV. q = 1.1 - 4.5, electron heat flux= 710^{-3} -310^{-2} MW/m^2). Left: gradient region. Right: central and edge regions.

IV. Interpretative and predictive simulation of ITB discharges at JET

An ITB discharge (#53521) combining LH power (2.7MW) with 15MW of NBI, 4MW of ICRH [14] has been analyzed using the package codes CRONOS. The electron ITB is maintained during the LH application. The ITB on the ion temperature, electron density and toroidal rotation profiles occurs at t=4.2s, and lasts during the whole high power phase (Fig. 3, left). Self-consistent calculation of the various non-inductive currents have been performed for this discharge. Current diffusion simulation well reproduced the evolution of the loop voltage, internal inductance, and Faraday rotation angles (Fig. 3, right). Simulations of ITBs

on T_e and T_i profiles are found to favor the modified mixed Bohm/gyro-Bohm model in Eq. (1) with magnetic shear (s) dependence by including a function $F(s) = \frac{1}{1+\exp(20(0.05-|s|))}$ in χ_e^B. Similar expression is used for ion transport: $\chi_i^{BgB} = 1.6\times 10^{-4}\chi_i^B F(s) + 1.75\times 10^{-2}\chi_i^{gB}$. Note that these formulas have been obtained from JET data. Good simulations of both the measured T_e and T_i profiles are shown in Fig. 4. However, the s dependence well reproduces the ITB for strong negative s value. For weak shear phase (t≥5s), the simulation of ITB sustainment requires the **ExB** shear effect [15]:

$$F(s) = \frac{1}{1+\exp(20(0.05+\omega_{ExB}/\gamma_{ITG}-|s|))},\ \gamma_{ITG} = 0.1\frac{c_s}{a}\left(\frac{a}{L_{ni}}+\frac{a}{L_{Ti}}\right)^{0.5}\left(\frac{T_i}{T_e}\right)^{0.5} \text{ [15]}$$

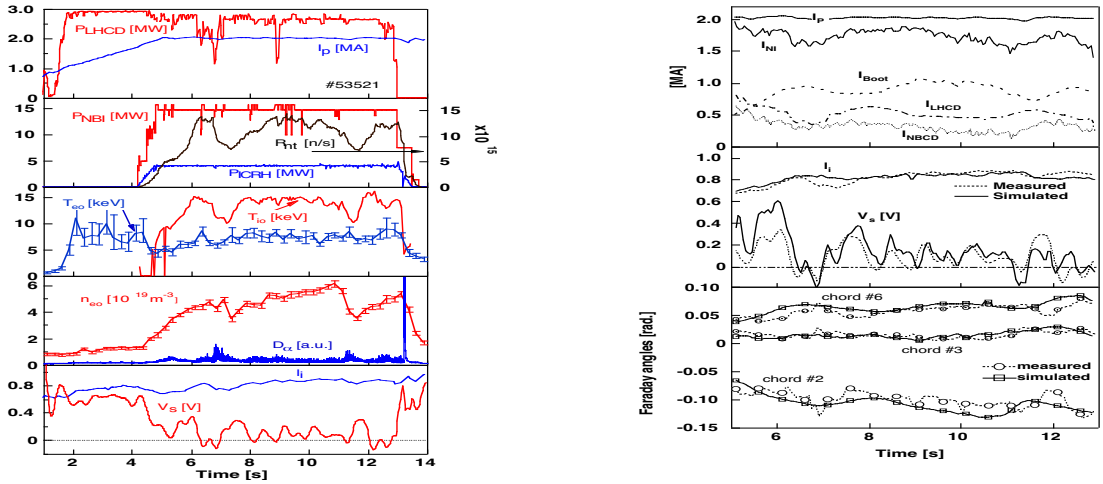

Fig. 3: Main parameters of JET discharge exhibiting ITBs (#53521). Left: additional powers (P_{LHCD}, P_{NBI}, P_{ICRH}), plasma current (I_p), neutron yield (R_{nt}), central ion/electron temperature (T_{io}, T_{eo}), central electron density (n_{eo}), D_a emission, internal inductance (l_i) and loop voltage (V_s). Right: interpretative simulation with CRONOS; non-inductive currents, sefl-inductance (li), loop voltage (V), and Faraday rotation angles (dashed: measurements, full: simulation).

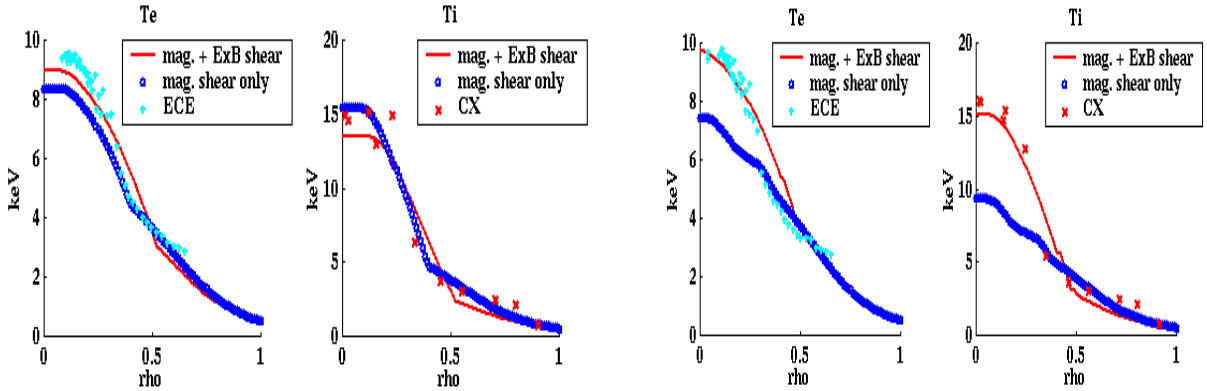

Fig. 4: Predictive simulation of JET discharge #53521 with mixed Bohm/gyro-Bohm model for weak (left, at t=5s) and strong negative magnetic shear (right, at t=8s).

V. Integrated predictive simulations of Tore Supra discharges with ETG transport

Purely predictive simulations of FWEH discharges on Tore Supra strongly favor the electromagnetic ETG model confirming the earlier indications of a good correlation of the

ETG model with the electron power balance data [5, 13]. Fig. 5 shows in the top, left panel the programmed FW power pulse for shot #TS18369, followed below by the evolution of the electron temperature at four radial positions compared with the theoretical model. The comparison for the total stored energy is given and is found in excellent agreement due to the reasonably good agreement of the radial profiles. On the right panel the comparison between the predicted and measured loop voltage also show good agreement. The polarimetry diagnostic measurement is given in the lower right hand panel. The integrated simulation codes predict the current profile penetration from which the poloidal magnetic field and total field angle are compared with those measured by the Faraday rotation diagnostic.

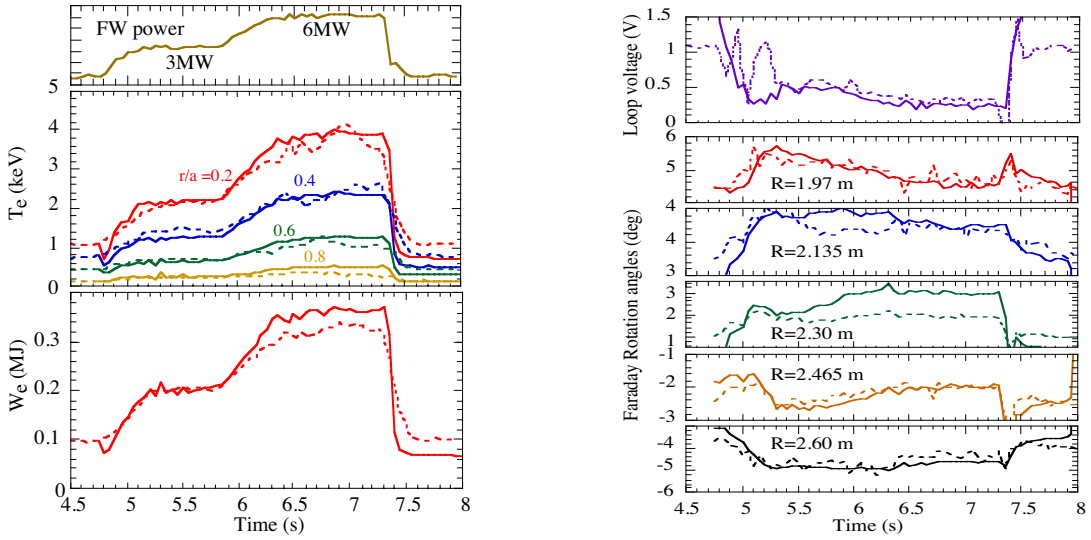

Fig. 5: Predictive simulation of Tore Supra FWEH discharge (#18368, Ip = 0.6 MA, B = 2.2T, $n_e(0) = 4x10^{19}m^{-3}$) with the ETG model in Eq. 3. (solid lines: simulations; dashed lines: measurements).

VI. Conclusion

Four transport models have been tested against the Tore Supra and JET experimental data. Mixed Bohm/gyro-Bohm formula, derived from JET database, well simulates the formation and sustainment of JET ITBs when including the magnetic and **ExB** shears in the Bohm term. ETG electron heat diffusivity explains and predicts the Tore Supra FWEH discharges as successfully as the empirical formulas. Good simulations of existing discharges with CRONOS improve the confidence in the predictions of such an integrated package of codes for predicting the achievement of steady-state plasmas, involving non-inductive current drive and feedback control.

References

[1] V. Basiuk, *et al*, 3rd IAEA Tech. Committee Meeting, Arles, France (2002), to be published in Nucl. Fusion.
[2] M. Erba, *et al*., PPCF, 39 (1997) 261.
[3] P. H. Rebut, *et al*., Phys. Fluids, B3, (1991) 2209.
[4] H. Nordman, J. Weiland, A. Jarmen, Nuclear Fusion **30**, 6 (1990) 983.
[5] W. Horton, *et al*,. Phys. Plasma 7 (2000) 1494.
[6] G. T. A. Huysmans, *et al*., CP90 Conference on Comp. Physics, Word Scientific Publ. Co. 1991, p.371.
[7] W. A. Houlberg, *et al*., Phys. Plasma **4** (1997) 3230.
[8] F. Imbeaux, Report EUR-CEA-FC-1679 (1999).
[9] Y. Feng, *et al*., Computer Physics communications 88 (1995) 161-172
[10] L. G. Eriksson, *et al*., Nuclear Fusion **33** (1993) 1037.
[11] P. Zerlauth, *et al*., note interne DRFC n° 1 278.
[12] V. Krivenski, *et al.*, Nucl. Fusion **25** (1985) 127.
[13] G.T. Hoang, *et al*., Phys. Rev. Lett. **87**(12), 125001-1 (2001).
[14] X. Litaudon, *et al.*, Proc. 16th IAEA Montreal, Vol 1 (Vienna) 669.
[15] V. V. Parail, *et al.*, Nuclear Fusion **39** (1999) 429.